Photoelectrons in the LHC chambers

Philipp Dijkstal

June 6, 2017

Contents

1 Introduction

This report describes how photoemission seeding is implemented in PyECLOUD, especially regarding the electron cloud buildup simulations for the LHC arcs. It is laid out which quantities are necessary as an input to the simulations and how they have to be specified. Some of them are derived from the theory of synchrotron radiation, others are material properties taken from published experiment data. Several papers concerning these measurements are presented and discussed, in order to arrive at those parameters that represent the best knowledge available.

Furthermore, possible changes to PyECLOUD are outlined, some of which have already been implemented and could get merged into the main branch of the code.

2 Photoelectrons in PyECLOUD

2.1 Input parameters

In PyECLOUD, photoelectrons are generated simultaneously with the beam charge. Figure 1 shows the related input parameters of the code, these are explained in more details in the following pages.

The quantity **k_pe_st** is the total number of photoelectrons per proton and m.
The quantity **refl_frac** is the ratio between all photoelectrons and those that origin from reflected photons.

The generation of photoelectrons created by immediately absorbed photons and reflected photons differs in PyECLOUD, see Fig. 2. For both of them, an angle relative to the center of the chamber is randomly generated. In the case of non-reflected photons, this angle is Gaussian distributed with a standard deviation of **a_limit**. In the case of reflected photons, an angle of reflection with respect to the impact point is obtained from a given distribution. The point where photoelectrons are generated is determined as the intersection of the line between a point on the outer circle and the origin with a chamber wall.

inv_CDF_refl_photoem_file includes the inverse cumulative distribution function (CDF) for the angles under which the photons are reflected from the impact point.

Photoelectrons are emitted with a truncated Gaussian energy distribution, specified by **e_pe_sigma** and **e_pe_max** with only positive energies allowed. Their initial direction is found through a cosine distribution for the angle with respect to the surface normal at these points.

out_radius describes a circle that encloses the beam chamber, see Fig. 2.

x_0_refl and **y_0_refl** are coordinates that have to be located inside the chamber. This point together with an angle of reflectivity leads to the positions of new MPs from reflected photons, see Fig. 2. Cases where y_0_refl is nonzero are not supported, yet.

Photoemission parameters (if the following input parameters are omitted primary electron generation by photoemission is not enabled).	
photoem_flag	(optional – default=0) (1 ⇒ On, 0 ⇒ Off) Enables primary electron generation by photoemission.
inv_CDF_refl_photoem_file	Name of a .mat file providing the inverse of the Cumulative Distribution Function (CDF) for the angular distribution of the reflected photons. If inv_CDF_refl_photoem_file = 'unif_no_file' the reflected photons have uniform angular distribution and no file needs to be provided.
k_pe_st	[m^{-1}] Number of photoelectrons to be generated per proton and per unit length.
refl_frac	Fraction of photoelectrons generated by reflected photons.
alimit	[rad] Extent of the angular (gaussian) distribution of photoelectrons generated by non-reflected photons.
e_pe_sigma	[eV] Width (1σ) of energy distribution (gaussian) of photoemitted electrons.
e_pe_max	[eV] Energy corresponding to the maximum of the energy distribution.
x0_refl, y0_refl	[m] Impact of non-reflected photons.
out_radius	[m] Radius of a circle external to the chamber.
phem_resc_fact	Rescaling factor on the position vector of the generated photoelectrons.

Figure 1: The input parameters of the PyECLOUD simulation code regarding photoemission seeding.

2.2 Validation

A script to generate the plots seen in Fig. 3 is part of the "photoemission" branch of PyECLOUD on GitHub ("test_photoemission.py"). It calls the photoemission module to produce these plots, and shows that the expected behavior is indeed achieved.

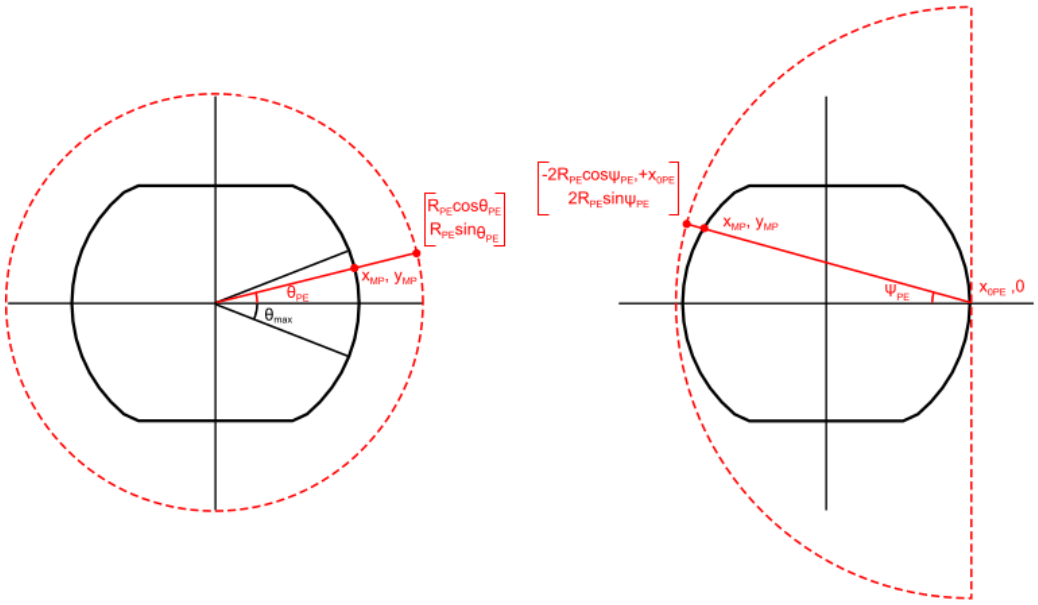

Figure 2: Position generation algorithm for photoelectrons from non-reflected (left) and reflected (right) photons [1].

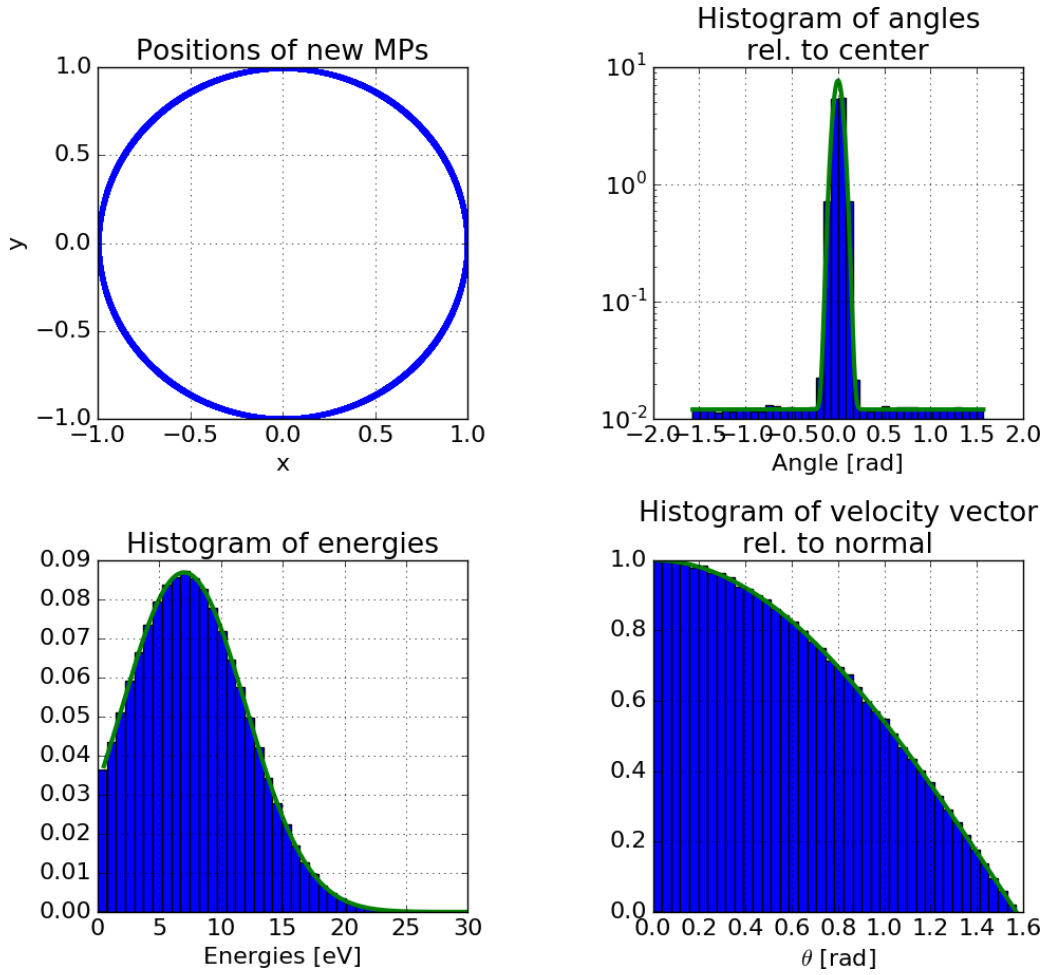

Figure 3: The photoemission seeding is validated with these tests. The top two plots show the positions of new macroparticles for a circular chamber. The green line is the expected behavior for an alimit of 0.05 and a refl_frac of 3.8%, given a uniform distribution of reflected photons. The bottom plots show the energies and angles relative to the impact normal for new macroparticles.

3 Photons emitted by the beam

To estimate the number of photoelectrons in the LHC beam pipe, the amount of photons generated by the beam has to be calculated first. The equations necessary for this were found in [2].

Eq. (5.40) in this reference describes the power spectrum of the radiation emitted by the beam.

$$\frac{\mathrm{d}P}{\mathrm{d}\omega} = \frac{P_s}{\omega_c} S_s(\frac{\omega}{\omega_c}) \tag{1}$$

P_s and ω_c are the total power emitted in the bend and the critical frequency of the radiation:

$$P_s = \frac{e^2}{4\pi\epsilon_0}\frac{2c\gamma^4}{3\rho^2} \tag{2}$$

$$\omega_c = \frac{E_c}{\hbar} = \frac{3c\gamma^3}{2\rho} \tag{3}$$

$$\frac{P_s}{\omega_c} = \frac{e^2\gamma}{9\pi\epsilon_0\rho} \tag{4}$$

An approximation here is $\beta \approx 1$, certainly fulfilled for any accelerator that emits significant synchrotron radiation. The function S_s is an integral over a modified Bessel function.

$$S_s(x) = \frac{9\sqrt{3}}{8\pi} x \int_x^\infty \mathrm{d}z'\ K_{5/3}(z') \tag{5}$$

The spectrum is easily transformed from frequency to number of photons with the relation $P(\omega) = \dot{n}\hbar\omega$. Integration yields the number of photons above a certain energy, for example the work function of the material of interest.

$$\frac{\mathrm{d}\dot{n}}{\mathrm{d}\omega} = \frac{P_s}{\omega_c}\frac{1}{\hbar\omega} S_s(\frac{\omega}{\omega_c}) \tag{6}$$

$$\dot{n} = \frac{P_s}{E_c}\int_{\omega_{\min}}^\infty \mathrm{d}\omega \frac{1}{\omega} S_s(\frac{\omega}{\omega_c}) \tag{7}$$

$$= \frac{P_s}{E_c}\int_{\omega_{\min}/\omega_c}^\infty \mathrm{d}x \frac{1}{x} S_s(x) \tag{8}$$

$$= \underbrace{\frac{P_s}{E_c}\frac{9\sqrt{3}}{8\pi}}_{=\frac{\sqrt{3}}{8\pi^2\hbar}\frac{e^2\gamma}{\epsilon_0\rho}} \cdot \underbrace{\int_{\omega_{\min}/\omega_c}^\infty \mathrm{d}x \int_x^\infty \mathrm{d}z' K_{5/3}(z')}_{=A(\omega_{\min}/\omega_c)=A(x_{\min})} \tag{9}$$

The double integral $A(\omega_{\min}/\omega_c)$ can be transformed into a single integral.

$$A(x_{\min}) = \int_{x_{\min}}^\infty \mathrm{d}x \underbrace{\int_x^\infty \mathrm{d}z'\ K_{5/3}(z')}_{=F(x)} \tag{10}$$

$$= \int_{x_{\min}}^\infty \mathrm{d}x\ F(x)\cdot 1 \tag{11}$$

$$= \underbrace{\lim_{b\to\infty} F(b)\cdot b}_{=0} - F(x_{\min})\cdot x_{\min} - \int_{x_{\min}}^\infty \mathrm{d}x\ F'(x)\cdot x \tag{12}$$

$$= -\int_{x_{\min}}^\infty \mathrm{d}x\ K_{5/3}(x)\cdot x_{\min} - \int_{x_{\min}}^\infty \mathrm{d}x\ (-K_{5/3}(x))\cdot x \tag{13}$$

$$= \int_{x_{\min}}^\infty \mathrm{d}x\ K_{5/3}(x)(x - x_{\min}) \tag{14}$$

The number of photons per m bend is obtained by applying a factor of $1/c$ to $\dot{n}$.

$$n_\gamma = \frac{\mathrm{d}n}{\mathrm{d}z} = \frac{\sqrt{3}}{8\pi^2}\frac{e^2\gamma}{\hbar c\epsilon_0\rho}\cdot\int_{\omega_{\min}/\omega_c}^{\infty}\mathrm{d}x\ K_{5/3}(x)(x-\frac{\omega_{\min}}{\omega_c}) \tag{15}$$

Another interesting feature is the angular distribution of photons. Far above the critical angle, emission of synchrotron radiation is negligible.

$$\theta_c(\omega) = \frac{1}{\gamma}\left(\frac{2\omega_c}{\omega}\right)^{1/3} = \left(\frac{3c}{\rho\omega}\right)^{1/3} \tag{16}$$

For energies corresponding to the copper work function, the critical angle is about 0.36 mrad.

Figure 4 shows the properties of some functions that were presented previously. It is created with a script found in a python module that is related to this report [3].

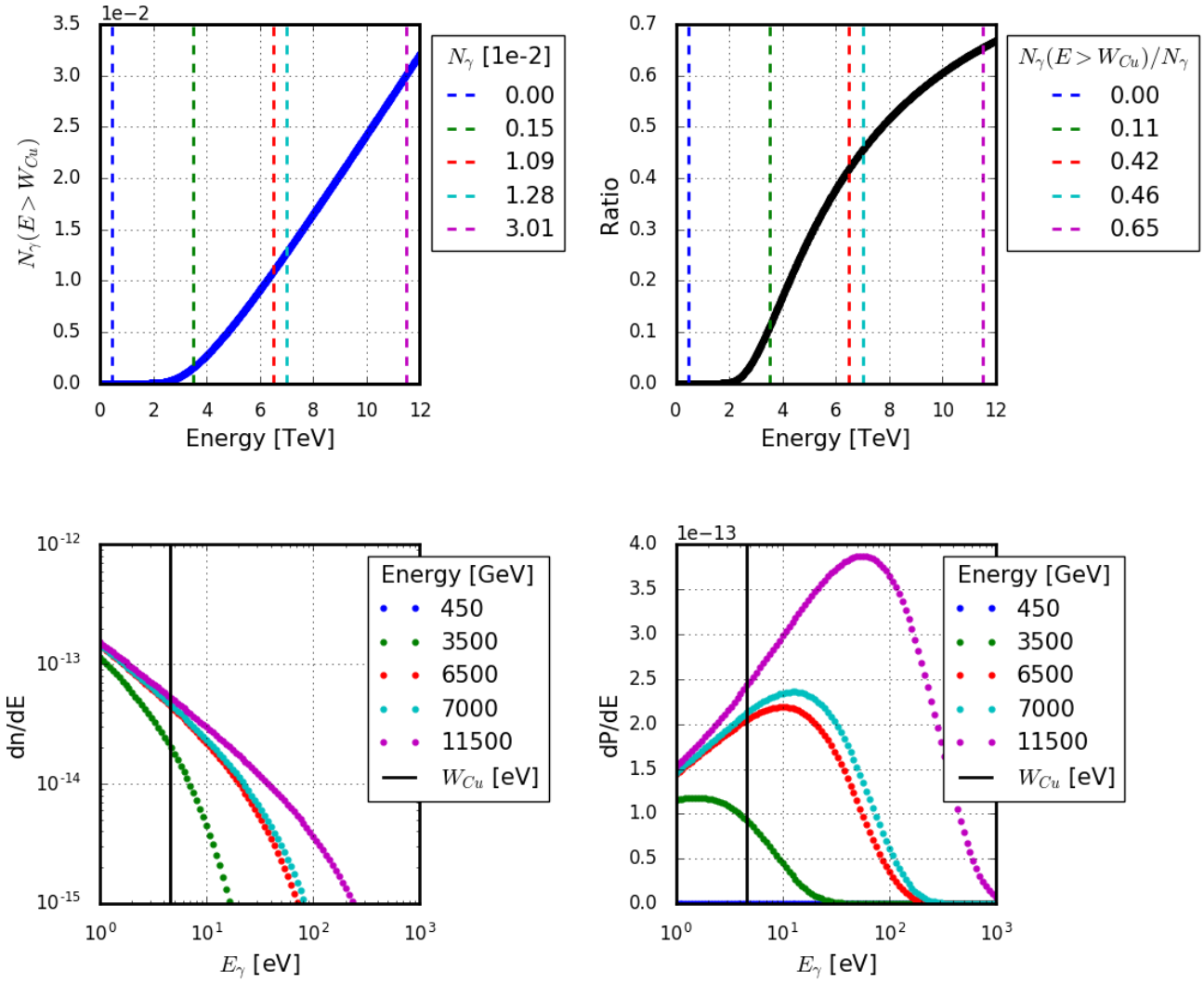

Figure 4: Top left: Number of photons above the copper work function in the LHC. Top right: Ratio of photons above the copper work function. Bottom left: Distribution of photons for various beam energies. Bottom right: Energy distribution of the impinging photon.

4 Distributions of photons in the LHC chamber

4.1 LHC chamber with sawtooth structure

The transverse geometry of the LHC chamber is pictured in Fig. 5. Of great importance is the sawtooth structure that ensures an almost normal impact of most photons on the surface, greatly reducing the reflectivity. Therefore, most photoelectrons are created at the outer part of the beam screens, where they do not significantly contribute to the electron cloud buildup.

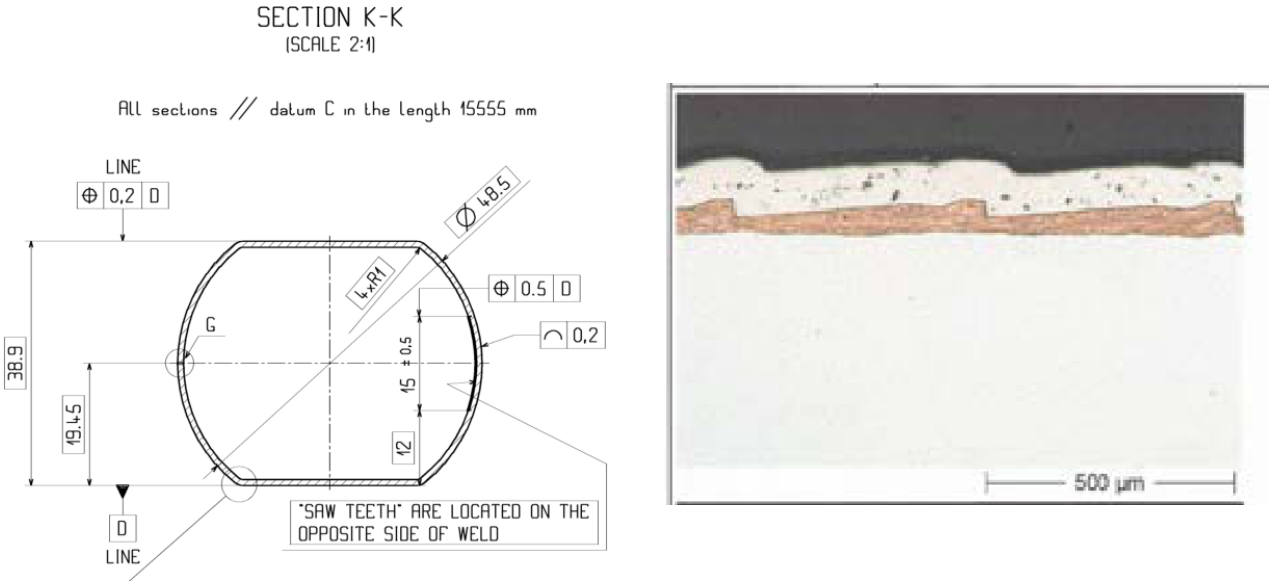

Figure 5: Left: the technical drawing of the LHC beam screen [4]. Right: a closeup of the sawtooth structure. The vertical edges are about 35 μm long [5].

4.2 SynRad3D simulations

The azimuthal distributions of absorbed photons in the LHC chamber have been simulated with the code SynRad3D [6]. The photons origin from a beam with 7 TeV energy, and only photons with more than 4 eV energy are considered. The results are shown in Fig. 6. With access to the raw data, it could be converted to the PyECLOUD input parameter **inv_CDF_refl_photoem_file**.

4.3 Other simulations

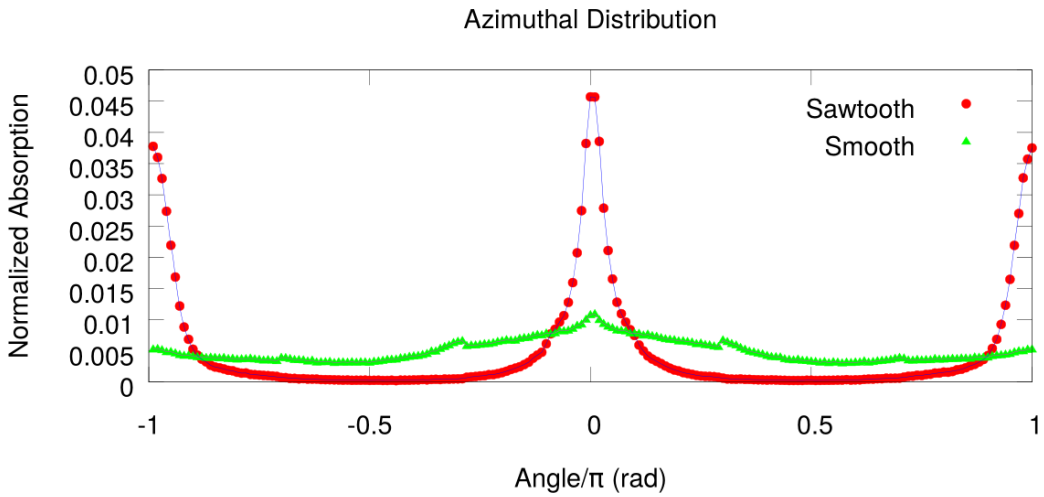

Figure 6: The photon distribution as it was simulated for the LHC chamber geometry with and without sawtooth [6]. An angle of 0 corresponds to the impact point of the synchrotron radiation.

5 Emission of photoelectrons from the LHC beam screen material

Several papers on relevant material properties are discussed in this section. The following notation is used in most of them

$$R = \frac{n_{\gamma,\text{reflected}}}{n_{\gamma,\text{incident}}} \tag{17}$$

$$Y = \frac{N_e}{n_{\gamma,\text{incident}}} \tag{18}$$

$$Y^* = \frac{N_e}{n_{\gamma,\text{absorbed}}} = \frac{Y}{1-R} \tag{19}$$

5.1 Baglin, Collins, Gröbner 1998 (CERN)

The properties of several materials, including co-laminated copper with and without sawtooth structure, were studied regarding photon reflectivity and photoelectron yield per photon [7].

5.1.1 Experiment setup

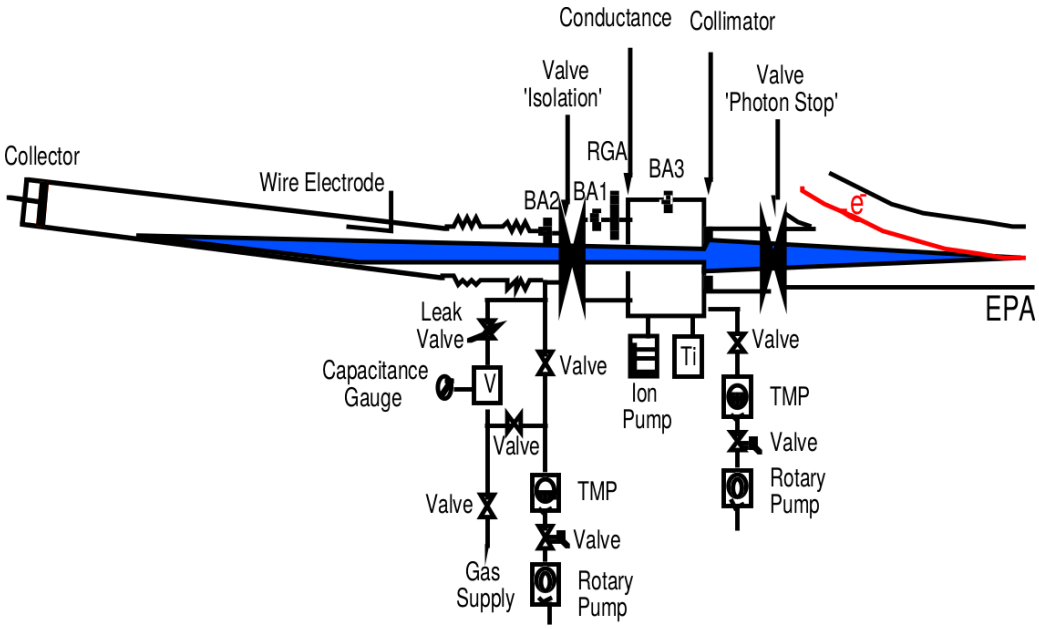

Figure 7: Experiment setup of the paper presented in Sec. 5.1.

Fig. 7 shows the experiment setup. It was possible to measure forward reflectivities and photoelectron yields. The collimator is of square geometry and 11 mm wide. The authors write:

> Due to the vertical collimation, photon energies below about 4 eV are attenuated.

The photoelectrons are measured at the collector, either after direct impact or after a reflection as shown in the figure. The ratio of the two currents is the photon reflectivity, where the backwards reflected photons are neglected (see Sec. 5.3).

The report cites that for radiation with a critical energy of 45 and 194 eV, corresponding to 7 and 11.5 TeV LHC beams, the number of photons is multiplied by 0.46 and 0.65, respectively. This exactly coincides with the ratio of photons above the work function with respect to all photons, see Fig. 4.

5.1.2 Results

The results of this paper are given in Fig. 8. Note that the photoelectrons per incident photon Y has been measured, which was then transformed to the photoelectrons per absorbed photon, Y^*. The reflectivity R was measured at an incidence angle of 11 mrad for the sample without sawtooth.

		45 eV		194 eV	
Surface	Status	R (%)	Y* (e/ph)	R (%)	Y* (e/ph)
Cu co-lam.	as-received	80.9	0.114	77.0	0.318
	air baked	21.7	0.096	18.2	0.180
Cu elect.	as-received	5.0	0.084	6.9	0.078
Cu sawtooth	as-received	1.8	0.053	-	-
	150°C, 9h	1.3	0.053	1.2	0.052
	150°C, 24h	1.3	0.040	1.2	0.040

Figure 8: The main results of the paper from Sec. 5.1, surface properties for different materials when radiated by two different photon distributions, characterized by the critical photon energy. R is the fraction of reflected photons, Y* the electron yield per absorbed photon.

5.1.3 Open questions

1. The authors claim that the photons were sent through a collimator with 11x11 mm size, leading to the photons below 4 eV to be attenuated. It is not clear how exactly the low energy photons were attenuated, or why this would have been necessary.
2. The photon induced scrubbing of the surface was not subject of this paper. The photon flux or integrated photon dose is not stated. The photoelectron yields that are quantified in this paper should probably be used as an upper limit.
3. Considering the paper from Sec. 5.3, the real reflectivity of the samples, especially with sawtooth, is expected to be higher. Because Y^* and R are not independent, Y^* should maybe be updated (increased) according to Eq. (19).

5.2 Baglin, Collins, Gröbner, Grünhagel et al. 2001 (CERN)

Photon-induced scrubbing is quantified with the same measurement apparatus as presented in Sec. 5.1 [8]. Again, co-laminated copper with and without sawtooth was subject of these studies, however only the results for the material with included sawtooth are fully reported.

5.2.1 Experiment setup

Copper samples can be irradiated by synchrotron radiation from EPA and their reflectivities and photoelectron yields can be measured in the same way as in Sec. 5.1. The sample consisted of a Cu sawtooth structure.

5.2.2 Results

Figure 9 shows the results from the measurements of this paper. There are clear differences in the reflectivity, which is much higher than in Fig. 8. They imply that the yield is much smaller and the reflectivity much higher than before. Furthermore they document the photon scrubbing after a dose of $1.5 \cdot 10^{22}$ photons, corresponding to about 600 h of LHC operations, as stated in the paper. After

this, the yield is about halved. However the full results indicate that this process would continue to decrease the yield even further, see Fig. 9. There seems to be no effect on the reflectivity.

	45 eV		194 eV	
Dose (ph/m)	R (%)	Y* (e/ph)	R (%)	Y* (e/ph)
~ 2 10^{19}	8	0.029	7	0.040
1.5 10^{22}		0.015		0.022

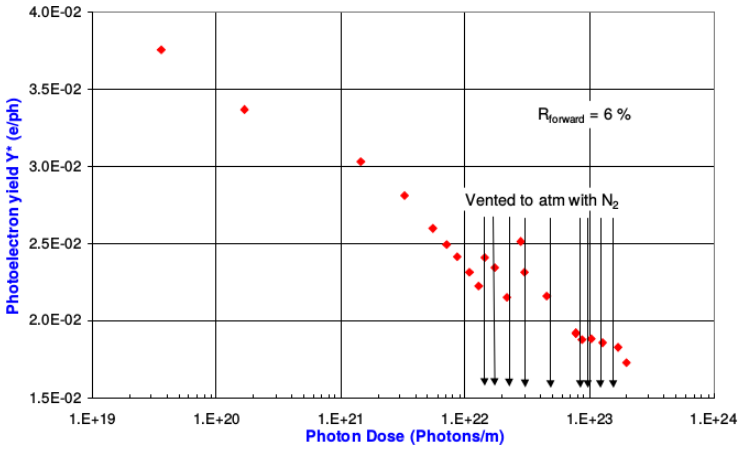

Figure 9: Left: the reflectivities and photoelectron yields from the measurements of Copper samples with sawtooth presented in Sec. 5.2.
Right: the impact of photon scrubbing on the photoelectron yield.

The differences to the paper discussed in Sec. 5.1, performed with the same experiment setup, is explained with the conditioning by reflected photons during the previous experiments.

5.2.3 Open questions

1. It is stated that Cu co-lam. without sawtooth has been subject to this study, yet the results are not published.

5.3 Mahne, Baglin, Collins et al. 2004 (ELETTRA)

This paper [9] covers only the photon reflectivity distributions, these were measured at ELETTRA, Italy.

5.3.1 Experiment setup

The experiment discussed in this paper is based on measured photons instead of electrons, see Fig. 10. Copper samples with and without sawtooth were irradiated with synchrotron light between 8 and 200 eV. The reflectivity of the samples were measured in different directions. The electron yields however could not be recorded.

5.3.2 Results

The main results are listed in Fig. 11. First, the reflectivity depending on the angle is shown for synchrotron radiation with a critical energy of 44 eV, similar to the previously discussed paper from Baglin et al. The difference is that not only the reflectivity in forward direction was measured, but in all directions. Figure 11 (bottom) specifies the total reflectivity. In case of the sawtooth, reflectivity increases from 1.8% to 10%.

Furthermore, it was found that the reflectivity depends on the photon energy. This means that also the spectrum of reflected photons is different from the original one.

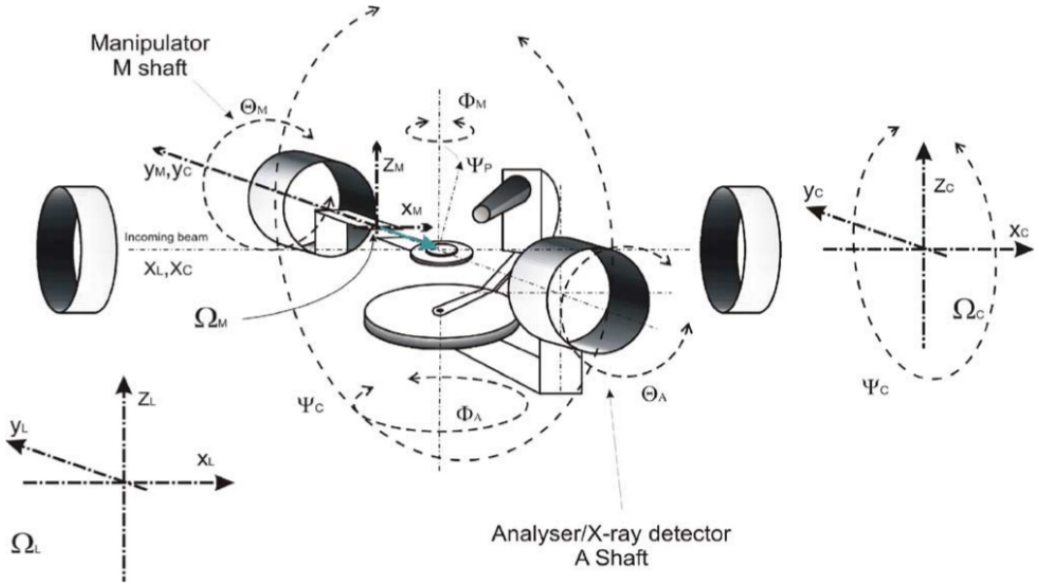

Figure 10: The experiment setup from Sec. 5.3.

5.3.3 Open questions

Some inconsistencies exist.

- The Baglin paper from Sec. 5.1 measured reflectivity as 1.8% for the sawtooth sample, whereas the forward scattering in this paper alone amounts to 4%.
- Furthermore, it is unclear how the 2% diffused photons are obtained from a white light spectrum. In Fig. 11 (right), the amount of diffused photons never reaches 2% for any photon energy. This discrepancy is not commented in the paper.
- The photon flux is not stated, photon scrubbing is not mentioned.

5.4 Cimino, Collins, Baglin 1999 (BESSY)

This very long paper [10] covers many interesting aspects.

- kinetic energy of photoelectrons
- angular spectrum of photoemission
- dependence of emission on photon energy
- photoemission yields
- impact of photon scrubbing on yields and kinetic energies

Many materials were studied, among those is Copper but without sawtooth structure.

5.4.1 Experiment setup

Potentially monochromatic synchrotron radiation is guided to the experimental station. The reflectivity is not measured or taken into account. This means that the yields correspond to photoelectrons per incident photons Y.

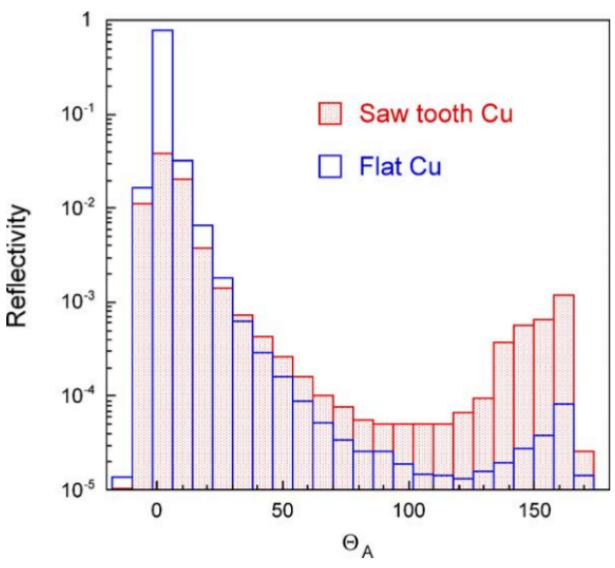

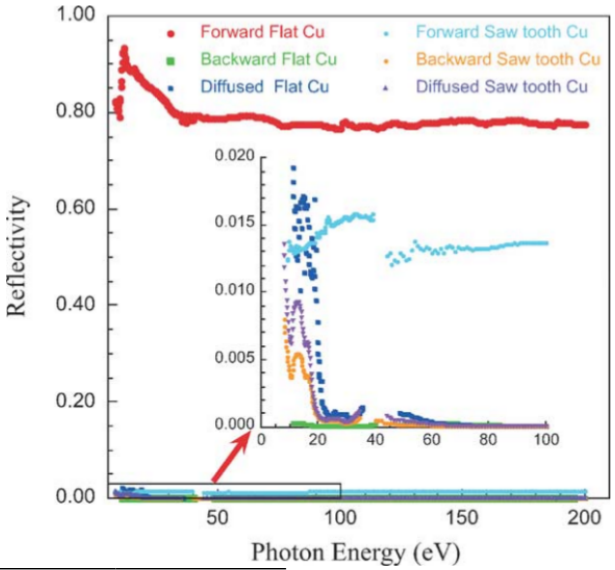

	Flat sample	Saw-tooth sample
Forward scattering (%)	80	4
Back scattering (%)	0	2
Diffused (%)	2	4
Total	82	10

Figure 11: Left: Measured reflectivity of Cu samples for different angles after grazing incidence. Right: Measured electron yield of Cu samples.
Bottom: Summary of reflectivities for a LHC-type spectrum from the paper presented in Sec. 5.3.

5.4.2 Results

The kinetic energy spectra of photoelectrons from Copper were measured before and after scrubbing with white light, see Fig. 13. It is notable that the photoelectron yields Y are much higher than those presented in Sec. 5.1. Regarding the spectra of kinetic energy, it becomes clear that white light scrubbing has a similar effect as surface cleaning with Argon sputtering. Especially the output of low energy photoelectrons is diminished, meaning that also the total yield decreases significantly.

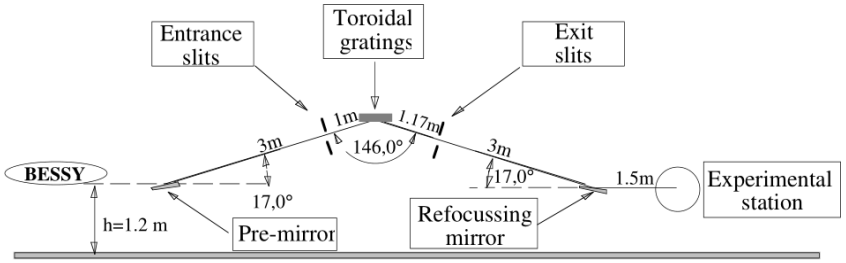

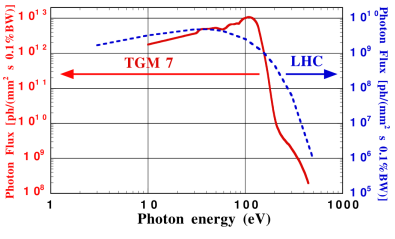

Figure 12: Left: The experiment setup for the paper presented in Sec. 5.4. Right: The white light spectrum of the SR source.

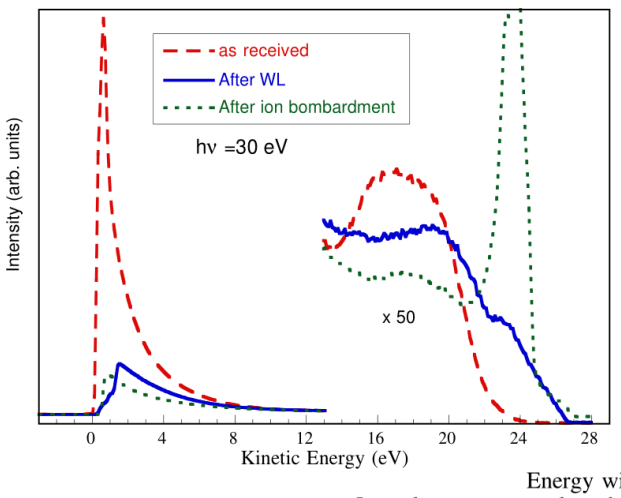

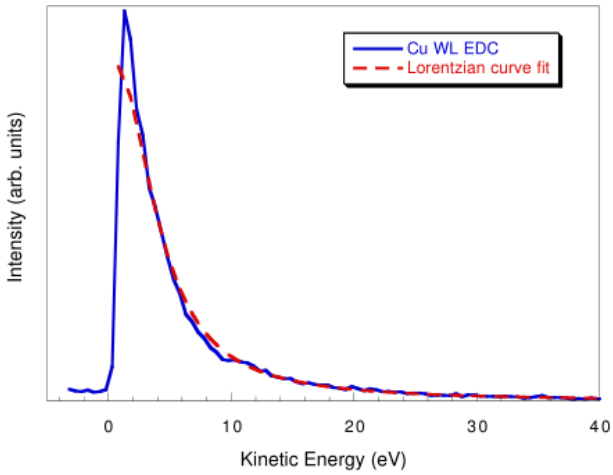

Sample	Low dose WL yield (electrons/photon)	Energy window low dose WL yield (electrons/photon)	WL yield (electrons/photon)	Energy window WL yield (electrons/photon)
Au	0.047 ± 0.020	0.022 ± 0.020	0.041 ± 0.002	0.023 ± 0.002
Cu	0.103 ± 0.020	0.051 ± 0.020	0.063 ± 0.002	0.042 ± 0.002

Figure 13: Left: The photoemission spectra for 30 eV photons on Copper (Sec. 5.4). The blue curve corresponds to a state after scrubbing has been performed, it is similar to the spectrum after a surface cleaning with ion bombardment.
Right: A Lorentzian fit to the low-dose WL spectrum centered at 0.64 eV and 3.7 eV wide.
Bottom: WL photoelectron yields for Au and Cu. The energy window corresponds to photoelectrons with energies between 1 and 6 eV. After WL scrubbing, the yield decreases by about 40%.

6 Proposed changes for PyECLOUD

6.1 Cosine Theta distribution

As mentioned in Sec. 2.1, the emission angle of photoelectrons in PyECLOUD follows a cosine distribution, defined by:

$$\frac{\mathrm{d}n}{\mathrm{d}\Omega} \propto \cos\theta \tag{20}$$

$$\mathrm{d}\Omega_{2D} = \mathrm{d}\theta \tag{21}$$

$$\mathrm{d}\Omega_{3D} = \sin\theta \ \mathrm{d}\theta \ \mathrm{d}\varphi \tag{22}$$

In PyECLOUD, the two-dimensional case is implemented even though the buildup process happens in 3D space. This leads to too small angles in average, see Fig. 14, and is a common error in 2D simulation codes [11]. It impacts the buildup simulations because it influences the time necessary for a photoelectron to reach the opposing wall of the chamber, and potentially be absorbed there. A branch on GitHub named "angle_cosine3" changes this behavior.

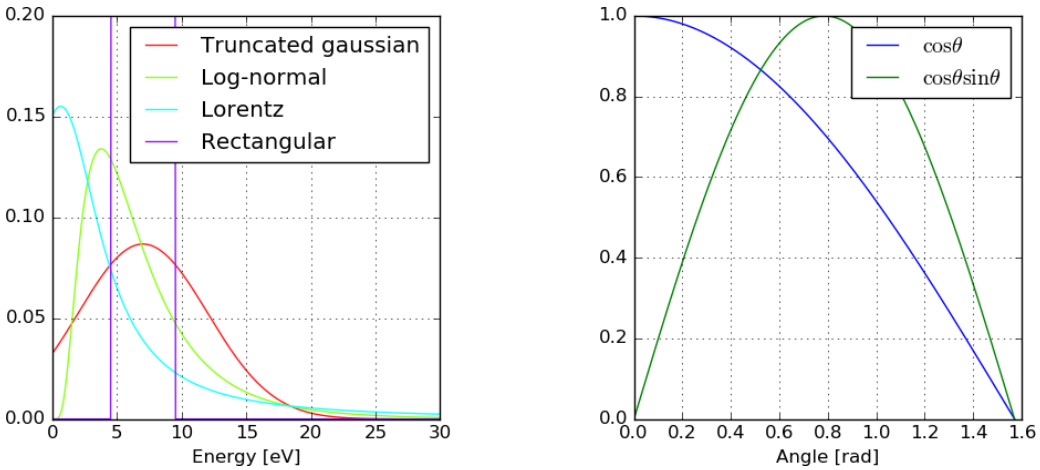

Figure 14: The left plot shows a cut-off normal distribution characterized by a width and a standard deviation. A log-normal distribution with the same mean and variance as the undistorted Gaussian distribution is shown in green. The log-normal distribution does not extend to negative values.

6.2 Energy of new photoelectrons

It would be possible to introduce a log-normal distribution for the energy of new macroparticles instead of a truncated Gaussian distribution. Such a log-normal distribution is also used in the case of new macroparticles from secondary emission multipacting in PyECLOUD. Alternatively, a truncated Lorentzian is suggested by the results shown in Fig. 13. Figure 14 visualizes these three approaches. A branch called "photoemission" on GitHub adds a new input parameter **energy_distribution**, the choices are in addition also a monoenergetic and a rectangular distribution.

6.3 Delayed photoelectron production

In PyECLOUD, photoelectrons are generated in parallel to the beam charge. This means that the difference in path length is not considered. Until a photon hits the chamber wall, the bunch has moved

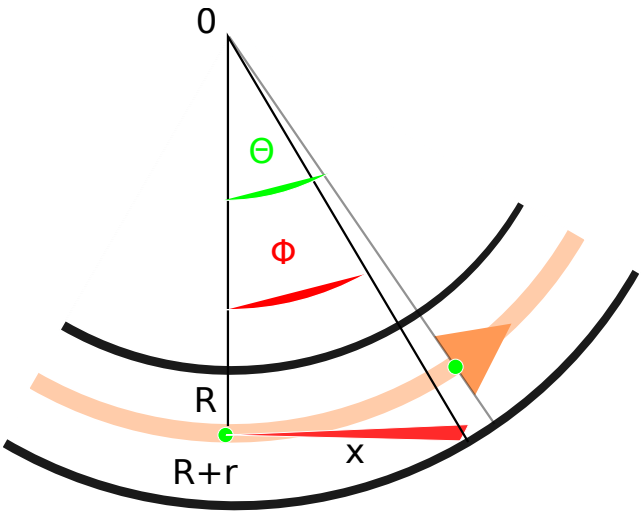

Figure 15: The path difference between protons (green) and photons(red).

further due to the bending, see Fig. 15. The path difference is calculated in the following way, where $R = 2803.95$ m for the LHC, and $r = 22$ mm. x is the distance travelled by the photons before the wall is reached.

$$(R+r)^2 = R^2 + x^2 \tag{23}$$

$$x = \sqrt{2Rr + r^2} = 11.1 \text{ m} \tag{24}$$

$$\Phi = \tan\frac{x}{R} = 0.00396136 \tag{25}$$

$$\Theta = \frac{x}{R} = 0.00396134 \tag{26}$$

$$\Delta t = \frac{R(\Theta - \Psi)}{c} = 1.938 \cdot 10^{-13}\ s \tag{27}$$

This path difference is negligible as it is much smaller than a time step in the simulation, normally around 10^{-11} s.

Furthermore, photons that are absorbed only after (multiple) reflections (note that the reflection coefficient for Copper without sawtooth is larger than 80%) are delayed with respect to the originating beam charge. One reflection in normal direction leads to a delay of $\Delta t = \frac{2r}{c} = 1.48{\cdot}10^{-10}$ s, insignificant with respect to the bunch spacing of $2.5 \cdot 10^{-8}$, but longer than a time step in the simulations.

6.4 Distribution of photoelectrons in the chamber.

Another idea would be to simulate the distribution of absorbed photons, and therefore the positions of new electron macroparticles. Currently, there is only a choice between a cosine and a uniform distribution of Ψ in Fig. 2 Based on the high reflectivity of the non-sawtooth parts of the LHC chamber, a uniform distribution might be the best approximation for the time being.

Figure 16 visualizes the time a photoelectron with a given energy and emission angle within the e-cloud stripes in a dipole needs to reach the opposing wall in absence of electric fields. In the currently used photoemission module of PyECLOUD this hardly makes a difference as photoelectrons are created simultaneously with the bunch charge and are therefore immediately accelerated. In case additional photoelectrons were created independent of time, or delayed with respect to the bunch, it may become relevant as low energy photoelectrons are more relevant because they do not reach the wall before the next proton bunch arrives and cannot get lost.

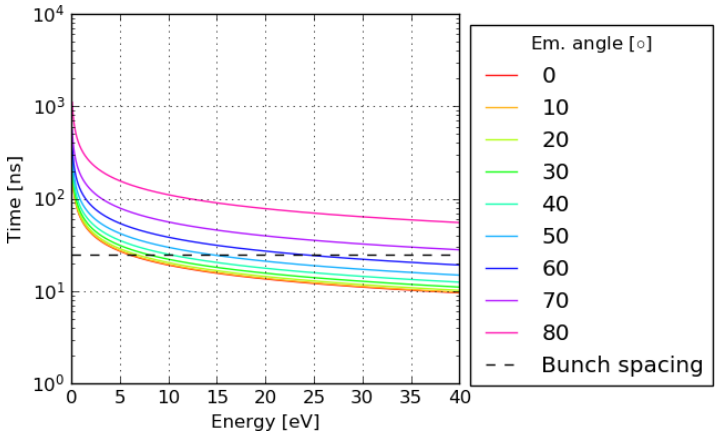

Figure 16: The time needed for a photoelectron in a dipole e-cloud stripe to reach the opposing wall in dependence of the emission angle relative to the surface normal and in absence of electric fields.

7 Best estimates for photoemission simulations

It is explained how the best estimates for the input parameters mentioned in Sec. 2.1 are defined based on the previously mentioned papers. Only some of them take photon induced scrubbing into account. The notation used in the following pages, see also Eq. (17-19):

Y_i (Y_i^*)	Photoelectrons per impinging (absorbed) photon on first impact
Y_r (Y_r^*)	Photoelectrons per impinging (absorbed) photon after initial reflection
R_i	Reflection rate of photons on first impact point.
R_r	Reflection rate of photons that have been reflected once.
N_i	Photoelectrons emitted on first impact of photons.
N_r	Photoelectrons emitted elsewhere.
N_t	Total number of emitted photoelectrons.
n_γ	Number of photons emitted per proton and m in a bending magnet.

7.1 Obtaining k_pe_st and refl_frac from measurements

In case of uniform material properties in the beam pipe, k_pe_st is computed as follows:

$$\mathbf{k\_pe\_st} = n_\gamma \frac{Y}{1-R} = N_\gamma Y^* \tag{28}$$

This is because all photons are eventually absorbed, either on direct impact or after an arbitrary number of reflections, and the material properties are uniform.

$$\mathbf{refl\_frac} = \frac{N_r}{N_i + N_r} = \frac{R_i Y_r^*}{(1-R_i)Y_i^* + R_i Y_r^*} \tag{29}$$

However in the case of the sawtooth configuration in the LHC beam screen, the material properties are different at the where the synchrotron radiation impacts first. This means that the reflectivity at this point plays a role, and the number of photons absorbed at the impact point and after initial reflection have to be weighted with the photoelectron yields Y^*.

$$\begin{aligned} \mathbf{k\_pe\_st} &= N_i + N_r && (30)\\ &= N_\gamma \left((1-R_i)Y_i^* + R_i Y_r^*\right) && (31)\\ &= N_\gamma \left(Y_i + R_i Y_r^*\right) && (32) \end{aligned}$$

One simplification is that photons are not reflected back to the sawtooth material, given its relatively small portion relative to the total circumference. This corresponds to $R_r = 0$. Quantitatively, k_pe_st and refl_frac are assessed in Sec. 7.3.

For **alimit**, the critical angle of the synchrotron radiation from Eq. (16) could be used for $\omega = W_{\mathrm{Cu}}/\hbar$: 0.36 mrad. For **e_pe_sigma** and **e_pe_max**, describing the kinetic energy distribution of new electron macroparticles, 5 and 7 eV have been chosen in past simulations. As stated before, the fact that photoelectrons are immediately being accelerated by the positively charged proton beam, means that their kinetic energy is of minor influence.

For the angular distribution of photoelectrons that are generated by reflected photons (**inv_CDF_ refl_photoem_file**), a uniform distribution should be used until a realistic distribution is not available. This approach should be better than using the cosine distribution, since the probability of multiple reflections is much higher than single reflection upon impact, since the reflectivity was measured to be larger than 80% for the non-sawtooth material. A 2D cosine distribution should in any case be avoided, see Eq. (22).

7.2 Consistency of different measurements

The different published experimental results on photoelectron yields and reflectivities are compared in this table. If two values are stated for a photoelectron yield, they correspond to the measurements before and after photon scrubbing. The reflectivities colored in red only include the forward reflectivity. The yields in blue were not published but could be retrieved with the simple relation between R, Y and Y^* from Eq. (19).

Source	Cu co-lam.			with sawtooth		
	R [%]	Y [e/ph]	Y^* [e/ph]	R [%]	Y [e/ph]	Y^* [e/ph]
Baglin 1998	80.9	0.022	0.114	1.8	0.052	0.053
Cimino 1999	-	0.103/0.063	-	-	-	-
Baglin 2001	-	-	-	8	0.021/0.011	0.029/0.015
Mahne 2004	82	-	-	10	-	-

The differences between the Cimino and Baglin results can be explained with different "as-received" samples of Cu. Since only the two Baglin papers include results for sawtooth materials, these should be used for the simulation. The reflectivities from the Mahne paper should be used because of the superior measurement apparatus for reflected photons.

7.3 Parameters to use for the simulations

For a **conservative estimate**, the following table uses the high reflectivities from the Mahne paper and the high photoelectron yields Y from the first Baglin paper, retrieved from the values for Y^* as published in [7].

Chamber type	R_i	R_r	Y_i	Y_r	Y_i^*	Y_r^*
Cu co-lam. with sawtooth	10.0	82.0	5.2e-02	2.2e-02	5.8e-02	1.2e-01
Cu co-lam.	82.0	82.0	2.3e-02	2.3e-02	1.3e-01	1.3e-01

These yields and reflectivities, together with the number of photons from Eq. (15), finally lead to the needed parameters refl_frac and k_pe_st.

Chamber type	N_i	N_r	N_t	n_γ	refl_frac	k_pe_st
Cu co-lam. with sawtooth	5.2e-02	1.2e-02	6.4e-02	1.1e-02	1.89e-01	7.00e-04
Cu co-lam.	2.3e-02	1.0e-01	1.3e-01	1.1e-02	8.20e-01	1.38e-03

A **realistic estimate** would include scrubbing effects and a much lower yield, as measured in the second Baglin paper. With respect to the first, the yield of the sawtooth material is by a factor of $0.052/0.011 \approx 4.7$ lower. If this factor is also applied to the yield of the other material, the following input parameters should be used. In practise, mostly the value for N_r is relevant as it denotes the amount of photoelectrons that contributes to the stripes in e-cloud simulations for dipoles and quadrupoles.

Chamber type	R_i	R_r	Y_i	Y_r	Y_i^*	Y_r^*
Cu co-lam. with sawtooth	10.0	82.0	1.0e-02	4.6e-03	1.1e-02	2.6e-02
Cu co-lam.	82.0	82.0	4.6e-03	4.6e-03	2.6e-02	2.6e-02

Chamber type	N_i	N_r	N_t	n_γ	refl_frac	k_pe_st
Cu co-lam. with sawtooth	1.0e-02	2.6e-03	1.3e-02	1.1e-02	2.03e-01	1.39e-04
Cu co-lam.	4.6e-03	2.1e-02	2.6e-02	1.1e-02	8.20e-01	2.81e-04

References

[1] G. Iadarola, Electron Cloud studies for CERN particle accelerators and simulation code development, Ph.D. thesis, University of Naples Federico II (2014).

[2] A. Hofmann, The Physics of Synchrotron Radiation, Cambridge University Press, 2004.

[3] python repository for pyecloud input paremeters.
URL `https://github.com/pdijksta/CellStudyInputPyECLOUD`

[4] CERN Technical Drawing LHCVSSB_0037.

[5] F. Zimmermann, Electron-Cloud Effects in past and future machines - walk through 50 years of Electron-Cloud studies, in: Proceedings, 5th Workshop on Electron-Cloud Effects (ECLOUD'12): La Biodola, Isola d'Elba, Italy, June 5-9, 2012, 2013.

[6] G. G. Cantón, D. Sagan, F. Zimmermann, Simulating Proton Synchrotron Radiation in the Arcs of the LHC, HL-LHC and FCC-hh, in: Proc. of International Particle Accelerator Conference (IPAC'16), Busan, Korea, May 8-13, 2016, 2016.

[7] V. Baglin, I. R. Collins, O. Gröbner, Photoelectron yield and photon reflectivity from candidate LHC vacuum chamber materials with implications to the vacuum chamber design, in: Particle accelerator. Proceedings, 6th European conference, EPAC'98, 1998., 1998.

[8] V. Baglin, I. R. Collins, O. Gröbner, C. Grünhagel, B. Henrist, N. Hilleret, B. Jenninger, Measurements at epa of vacuum and electron-cloud related effects, 2001, 11th Chamonix - LHC Workshop.

[9] N. Mahne, V. Baglin, I. Collins, A. Giglia, L. Pasquali, M. Pedio, S. Nannarone, R. Cimino, Photon reflectivity distributions from the LHC beam screen and their implications on the arc beam vacuum system, Applied Surface Science 235 (1–2) (2004) 221 – 226, 8th European Vacuum Conference and 2nd Annual Conference of the German Vacuum Society.

[10] R. Cimino, V. Baglin, I. Collins, Vuv synchrotron radiation studies of candidate lhc vacuum chamber materials, Vacuum 53 (1) (1999) 273 – 276.

[11] J. Greenwood, The correct and incorrect generation of a cosine distribution of scattered particles for monte-carlo modelling of vacuum systems, Vacuum 67 (2) (2002) 217 – 222.